Eur. Phys. J. B (2017) 90: 40
DOI: 10.1140/epjb/e2017-70531-0

THE EUROPEAN PHYSICAL JOURNAL B

Regular Article

On features of magnetization self-organization in 1D stochastic ferromagnetic systems

Anatoly A. Ivanov[1] and Vitaly A. Orlov[1,2,3,a]

[1] Siberian Federal University, pr. Svobodny 79, 660031 Krasnoyarsk, Russia
[2] Kirensky Institute of Physics Federal Research Center KSC Siberian Branch Russian Academy of Sciences, 660036 Krasnoyarsk, Russia
[3] Krasnoyarsk State Pedagogical University named after V.P. Astafev, ul. Ady Lebedevoi 89, 660049 Krasnoyarsk, Russia

Received 11 September 2016 / Received in final form 18 January 2017
Published online 8 March 2017 –

Abstract. The magnetic structure of a polycrystalline nanowire at the weak or missing magnetostatic interaction exhibits the special self-organization of magnetization. As is known, the magnetization structure forming in a random crystallographic anisotropy field has a characteristic length range, which involves tens and hundreds of crystallites. This leads to the occurrence of stochastic domains. The induced uniform anisotropy of magnetostatic nature or the texture co-directed with the crystallite anisotropy axes masks the picture of stochastic domains. Nevertheless, as we show, the information on stochastic domains remains in the magnetization structure. The experimental techniques for obtaining information on the magnetic properties of stochastic domains are proposed.

1 Introduction

The phenomenon of self-organization in the energy flux, which is accompanied by the occurrence of ordered structures at the random energy arrangement (Bernard cell, lasers, Belousov-Zhabotisky reaction, column structure of basalts, etc.), has evoked physical imagination. In all the observed situations, the competing factors (chaos and one-dimensional ordering) come into play. For instance, in the Bernard cell, the chaos is heat motion of liquid molecules and the ordering factor is the uniform temperature gradient in a homogeneous field of gravity. In the well-known self-organization manifestations, the external evidence is remarkable: ordered structures arise against the background of chaos.

Recently, there has been a keen interest in studying relatively new magnetic objects – ferromagnetic nanowires – with self-organization elements in the structure. In particular, the authors of [1,2] demonstrated the simplest case of magnetization self-organization in a nanowire bunch under the action of demagnetizing fields. The result observed was quite expected: neighboring nanowires appeared oppositely magnetized. The phenomenon of self-organization of the structures was observed in many systems containing the factor responsible for ordering: in systems of electric [3] and magnetic dipoles [4], superconductors [5], and thin ferromagnetic films [6–8]. In addition, it is interesting to consider the magnetization self-organization processes in 1D systems (nanowires and nanostripes) [9,10]. In particular, Rougemaille and Schmid [9] studied the formation of an ordered domain structure in wires with a diameter of a few atomic layers depending on the fabrication technique used.

In this work, we investigate the unusual self-organization type, specifically, the occurrence of the stochastic magnetization superstructure in a polycrystalline 1D ferromagnet. We consider a polycrystalline nanowire with a crystallite size somewhat smaller than the domain wall thickness (tens of nanometers). The crystallite easy magnetization directions are randomly distributed over a sphere. The exchange coupling between neighboring crystallites and crystallographic anisotropy of individual crystallites compete in the magnetic structure formation. The exchange coupling tends to uniformly distribute the magnetization, while the local anisotropy tends to create the random magnetization distribution. The magnetization field in the absence of the uniform macroscopic anisotropy is a conglomerate of the so-called stochastic domains (SDs) or magnetic blocks (MBs) [11–14]. The occurrence of the new length δ_S corresponding the SD size was detected in real experiments by different authors using different experimental tools [15–17].

Let us consider in more detail the magnetic properties of SDs. Ferromagnetic crystallites forming a wire exhibit the random orientation of local easy magnetization axes (EMAs) and, generally speaking, the spread in size, shape, and magnetic constants. The crystallites are so small that the inequality $a \ll \delta_0$ can be considered valid, where a

[a] e-mail: orlhome@rambler.ru

is the crystallite size and $\delta_0\sqrt{A/K}$ is the domain wall size in a homogeneous material (A and K are the exchange and anisotropy constants, respectively). Since the parameter a is small, the coordinate dependence of the magnetization $\mathbf{m}(\mathbf{r})$ inside a crystallite can be considered weak. When solving the linearized Landau-Lifshitz equation for $\mathbf{m}(\mathbf{r})$ at the crystallite width, we limit the consideration to the terms of the second order of smallness. This allows us to obtain the function $\mathbf{m}(\mathbf{r})$ in the quadratic approximation [18]. The obtained $\mathbf{m}(\mathbf{r})$ distribution is used to express the magnetic energy of a crystallite, which is represented by a function of magnetization direction angles at the grain boundaries, including polar angle ϑ and azimuth angle ϕ. The total energy $E(\vartheta_1 \dots \vartheta_{N+1}, \phi_1 \dots \phi_{N+1})$ of a magnet is the sum of energies of all crystallites. This completes the first stage.

At the second stage, we minimize the total energy E relative to the polar angle ϑ_n and azimuth angle ϕ_n of the magnetization at the crystallite boundaries and arrive at the system of equations

$$\frac{\partial E}{\partial \vartheta} = 0, \qquad \frac{\partial E}{\partial \phi} = 0. \tag{1}$$

In the expression for energy E, we took into account the exchange energy inside a crystallite and between crystallites, anisotropy energy, Zeeman energy, and energy of magnetostatic interaction between crystallites in the dipole approximation.

System of equations (1) was numerically solved using different techniques, including the gradient descent [18], field descent [19], and shootings [20]. These methods simulated the real experiment; in all cases, the characteristic length δ_S was determined, which is the SD linear size.

Now, let us consider a computer experiment for observing the presence of SDs in the magnetization structure. First, we exclude the macroscopic uniform anisotropy from the expression for the magnetic energy. We apply an external magnetic field perpendicular to the wire axis OZ, which magnetizes the nanowire to saturation. Then, the field is quasistatically decreased to zero. After that, the procedure is repeated in an external field rotated around the OZ axis by a certain angle. Repetition of the procedure at small rotations of the external magnetic field at gradual decreasing to zero leads to the initial configuration. However, at certain magnetic field and rotation angle values, the magnetization of some part of the neighboring crystallites does not return to the initial position. The wire part appears switched. Figure 1 shows the characteristic case of the magnetization switching by a rotating field [21,22]. One can see two mechanically stable magnetization angle distributions obtained at the same EMA directions. Vast magnetization regions containing tens or hundreds of coherently switched crystallites arise in the structure. These regions behave as independent formations, which almost do not interact with one another, and are called stochastic domains (SDs). The SD sizes are random values. The mathematical simulation shows that the possible sizes run the values from tens to hundreds of crystallite sizes. The SDs are characterized by their own induced anisotropy.

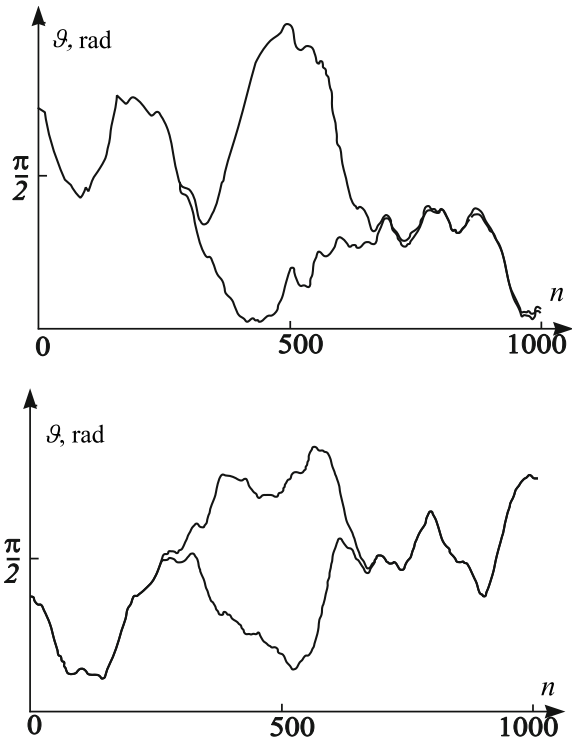

Fig. 1. Numerically simulated characteristic distributions of the polar and azimuth angles of magnetization along the wire upon switching by the rotating field. The numbers of crystallites are plotted on the abscissa axis.

2 Induced stochastic anisotropy

The magnetization distribution pattern shows that the occurrence of coherently switched regions can be considered as the manifestation of self-organization. This statement is grounded not only on the magnetic structure geometry, but on deeper manifestations. The SDs exhibit the pronounced uniaxial anisotropy [14] with its effective constant and effective axis direction.

To calculate the effective anisotropy constant for a block, we write the torque from the side of the random anisotropy field of an ensemble of crystallites contained in the SD. For the sake of simplicity, this calculation can be made with regard of the fluctuations of crystallites volumes and local anisotropy constants. Assuming the magnetization variation inside a SD to be minor and specified by the angle ϑ, we obtain the torque around the axis perpendicular to OZ:

$$M_\vartheta = \frac{\partial}{\partial \vartheta} \sum_{n=1}^{N} v_n K_n \left(\mathbf{m}_n \mathbf{e}_n\right)^2 = 2 \sum_{n=1}^{N} v_n K_n \left(\mathbf{m}_n \mathbf{e}_n\right) \frac{\partial \left(\mathbf{m}_n \mathbf{e}_n\right)}{\partial \vartheta}. \tag{2}$$

Here, v_n and K_n is the volume and local anisotropy constant for the nth crystallite, $\mathbf{e}_n$ are the EMA direction orts, and N the number of crystallites in a SD. The same torque should be induced by the effective anisotropy

of the SD that involves the block crystallites. We can write the effective anisotropy torque as

$$M_{\vartheta_{ef}} = \frac{\partial}{\partial\vartheta} V K_{ef} \left(\mathbf{m}\mathbf{e}_{ef}\right)^2 = 2V K_{ef} \left(\mathbf{m}\mathbf{e}_{ef}\right) \frac{\partial \left(\mathbf{m}\mathbf{e}_{ef}\right)}{\partial\vartheta}. \tag{3}$$

Here, K_{ef} and $\mathbf{e}_{ef}$ are the effective anisotropy constant and effective anisotropy axis (EAA) direction vector of the block, and $V = \sum v_n$ is the block volume. We equalize expressions (2) and (3) and obtain

$$\sum_{n=1}^{N} v_n K_{ef} \left(\mathbf{m}\mathbf{e}_{ef}\right) \frac{\partial \left(\mathbf{m}\mathbf{e}_{ef}\right)}{\partial\vartheta} = \sum_{n=1}^{N} v_n K_n \left(\mathbf{m}_n \mathbf{e}_n\right) \times \frac{\partial \left(\mathbf{m}_n \mathbf{e}_n\right)}{\partial\vartheta}. \tag{4}$$

Representation the scalar products in this expression via polar and azimuth magnetization angles, we obtain the effective constant

$$K_{ef} = \left[\frac{\left\langle K^2 \right\rangle - \mu^2 \left\langle K \right\rangle^2}{N} \left(\sigma_v^2 + 1\right) + \mu^2 \left\langle K \right\rangle^2 \right]^{\frac{1}{2}}. \tag{5}$$

Here, we introduced $\mu = \langle \cos(2(\alpha_n - \alpha_m)) \rangle$, crystallite EMA polar angle α, and dimensionless crystallite volume dispersion. The angular brackets indicate averaging over the ensemble.

Expression (5) is universal. It allows calculating the effective constant of a magnetic block for the two- and three-dimensional models (not only for nanowires) in the arbitrary directions of local axes, including the orientational texture, and local constants and volumes of crystallites, including those for periodic structures [23,24]. In the simple case of the uniform distribution of the crystallite local anisotropy axes directions over a sphere, expression (5) is simplified and acquires the form

$$K_{ef} = \frac{1}{V} \sqrt{\frac{1}{3} N \left\langle v^2 \right\rangle \left\langle K^2 \right\rangle}. \tag{6}$$

It should be noted that when the volumes and constants K of crystallites are identical, expression (6) acquires the well-known form $K_{ef} \approx K/\sqrt{N}$.

3 The occurrence of a superstructure

In the mechanism of the occurrence of a superstructure, the special role is played by the exchange coupling. The exchange extracts a certain mode, which manifests itself as a stochastic or magnetic domain, from the random picture of the easy anisotropy axes distribution. To under-stand the mechanism of SD nucleation, below we semi-qualitatively analyze the occurrence of the induced stochastic anisotropy.

To study the features of the distribution of the SD effective easy axes directions, we return to equation (4). Using this equation, we obtain the expression for the effective direction of the anisotropy axis

$$\sin(2\alpha_{ef}) = \frac{K}{K_{ef}} \sum_{n=1}^{N} \sin(2\alpha_n) = s_0. \tag{7}$$

Let us calculate the density of distribution of the quantity $s = \sin(2\alpha_{ef})$, which can be presented in the form

$$\rho(s) = \int_{-\alpha_0}^{\alpha_0} \dots \int_{-\alpha_0}^{\alpha_0} \prod_{n=1}^{N} \rho(\alpha_n) \delta(s - s_0) d\alpha_n. \tag{8}$$

Here, $\rho(\alpha_n)$ is the density of distribution of the EMA polar angles. For simplicity, assume this function to be independent on the crystallite number and α_0 to be a half of the polar angle of cone opening in the EMA distribution. In expression (8), the δ-function excludes the implementations α_n that do not satisfy condition (7) from integration. To obtain the final form of (8), we use the refining technique described in [25]. Further calculations suggest the identical multiplying of the density $\rho(s)$ by the exponential factor with the fitting parameter β and subsequent expansion in the Fourier integral:

$$\begin{aligned} \Omega(\xi) &= \int_{-\infty}^{\infty} \rho(s) \exp(\beta s) \exp(I\xi s) ds \\ &= \int_{-\infty}^{\infty} \int_{-\alpha_0}^{\alpha_0} \dots \int_{-\alpha_0}^{\alpha_0} \exp(\beta s + I\xi s) \\ &\quad \times \prod_{n=1}^{N} \rho(\alpha_n) \delta(s - s_0) d\alpha_n ds. \end{aligned} \tag{9}$$

The presence of the δ-function in the integrand of expression (9) after integration over s allows us to present the multiple integral as a product of identical single integrals

$$\begin{aligned} \Omega(\xi) &= \prod_{n=1}^{N} \int_{-\alpha_0}^{\alpha_0} \rho(\alpha) \exp\left((\beta s + I\xi s) \frac{K}{K_{ef}} \sin(2\alpha) \right) d\alpha \\ &= \omega(\xi, \beta, \alpha_0)^N. \end{aligned} \tag{10}$$

Here,

$$\omega(\xi, \beta, \alpha_0) = \int_{-\alpha_0}^{\alpha_0} \rho(\alpha) \exp\left((\beta s + I\xi s) \frac{K}{K_{ef}} \sin(2\alpha) \right) d\alpha.$$

The function $\omega(\xi, \beta, \alpha_0)$ is localized by parameter ξ and the main contribution is made by long-wavelength harmonics with small numbers ξ. We expand $\omega(\xi, \beta, \alpha_0)$ in the series over the smallness degrees ξ of up to the second order:

$$\ln(\omega(\xi, \beta, \alpha_0)) \approx \ln(\omega_0) + \left. \frac{\partial \ln(\omega(\xi, \beta, \alpha_0))}{\partial \xi} \right|_{\xi=0} \xi + \frac{1}{2} \left. \frac{\partial^2 \ln(\omega(\xi, \beta, \alpha_0))}{\partial \xi^2} \right|_{\xi=0} \xi^2. \tag{11}$$

Then, equation (10) acquires the form

$$\Omega(\xi) = \omega_0^N \exp\left(I s_{mid}\xi - \sigma^2\xi^2\right). \tag{12}$$

Here, we introduced the designations

$$s_{mid} = N\frac{\partial \ln(\omega(\xi,\beta,\alpha_0))}{\partial(I\xi)}\bigg|_{\xi=0},$$
$$\sigma^2 = \frac{N}{2}\,\frac{\partial^2 \ln(\omega(\xi,\beta,\alpha_0))}{\partial(I\xi)^2}\bigg|_{\xi=0}. \tag{13}$$

After the backward transformations, we arrive at

$$\rho(s) = \frac{1}{2\pi}\exp(-\beta s)\int_{\alpha_0}^{\alpha_0}\exp(-I\xi s)\Omega(\xi)d\xi. \tag{14}$$

The maximum accuracy of the calculation of expression (14) is attained at the fitting parameter β at which the current s value coincides with the average s_{mid} value. Consequently, under the condition $s = s_{mid}$, the desired distribution has the form

$$\rho(s) = \frac{\omega_0^N}{\sqrt{2\pi\sigma^2}}\exp(-\beta s). \tag{15}$$

As an example of using equation (15), we consider the interesting particular case of the uniform distribution of the EMA polar angle in the range from $-\alpha_0$ to α_0. In this case, we have $\rho(\alpha) = 1/(2\alpha)$. Taking this into account, we calculated expressions (13) and determined the β value using equation (15). It should be emphasized that at the complete chaos in the EMA directions $(-\pi/2 \ldots + \pi/2)$, the calculation with the use of equation (15) yields the correct limit case of the uniform distribution of the effective axes directions. Upon narrowing of the cone, the direction $\alpha_{ef} = 0$ is implemented more often. For the narrow cone ($\alpha_0 \ll 1$), the Gaussian approximation ($\beta = 0$) is satisfactory [26].

To experimentally determine the distribution function for the effective anisotropy axes for verifying relations (15), we can use an experimental technique similar to that described in Introduction, i.e., the rotating field technique. For this purpose, the external field angles at which the magnetization in a block changes its direction should be detected, since this event occurs when the field appears perpendicular to the effective axis of a block. If angle ε is the field application angle at which the magnetization jump occurs in the block, then the distribution density $\rho^*(\varepsilon - \pi/2)$ is the density of distribution of the effective axes. To ensure correctness of the comparison between the theory and experiment, the latter should involve, along with fixing the field angles, determination of the fitting parameter, i.e., the average number N of crystallites in a domain, which enters the expression for dispersion. The computer experiment carried out with regard of the aforesaid for several EMA misorientations showed very good agreement between the numerically calculated distributions of the effective anisotropy axes and the analytical calculation using equation (15).

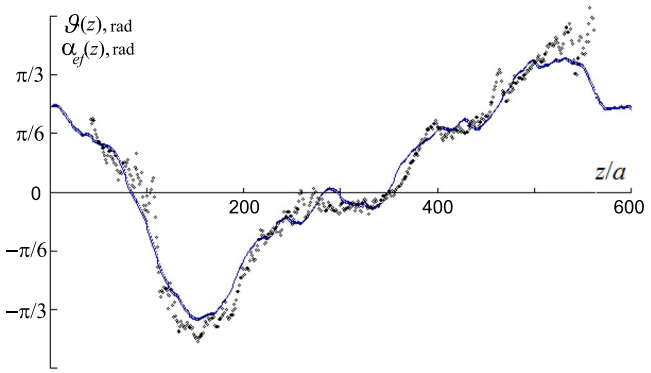

Fig. 2. Example of the magnetization distribution in a one-dimensional material with the randomly distributed EMA directions (solid line) in comparison with the effective axes directions deter-mined using the moving averaging technique.

In the context of the idea about the nature of anisotropy in stochastic magnets, it seems reasonable to attribute the magnetization field structure to the stochastic anisotropy structure, yet not with the local one. To clarify this correlation, the fluctuations of the effective anisotropy axes for crystallite groups in a sample were numerically studied. Here, the main idea was that the magnetization at each point of a sample is affected by the field of anisotropy closest to this place in the region with characteristic size δ_S. For each sample point, the direction of the effective anisotropy axis in the closest vicinity containing N crystallites was calculated using equation (4). Thus, the first block involved crystallites from the first to Nth; the second block, from the second to $(N+1)$th; the third block, from the third to $(N+2)$th, and so on. This technique for determining the directions of the effective block axes was latter called the moving averaging. For the same implementation of the EMA directions, the magnetization configuration $\vartheta(z)$ was built. After that, $\alpha_{ef}(z)$ and $\vartheta(z)$ were compared. The degree of coincidence of the dependences $\alpha_{ef}(z)$ and $\vartheta(z)$ strongly depends on the averaging range N. As a coincidence criterion, the average squared difference $\Delta = \sum_n(\vartheta_n - \alpha_{ef})^2/N$ was chosen. The N_S value was determined at which the Δ value is the smallest. Figure 2 shows magnetization configurations (solid lines) and distributions of the effective anisotropy axes (dots) to illustrate the correlation between the magnetization directions and SD effective anisotropy axes directions.

Note that the magnetization rotation dispersion within a SD cubically depends on the coordinate z, as in the models where the magnetization was not allowed to get out the plane [14]. Consequently, the functional dependence of the linear sizes of magnetic blocks on the crystallite parameter $b = a/\delta_0$ remains invariable:

$$\delta_S = \delta_0\left(\frac{12}{b}\right)^{\frac{1}{3}}. \tag{16}$$

Then,

$$N_S = \frac{\delta_S}{a} \approx \left(\frac{12}{b^4}\right)^{\frac{1}{3}}. \tag{17}$$

The N_S value calculated using equation (17) agrees well with the SD sizes from the computer experiment. Since the fluctuations of the magnetization field of an inhomogeneous magnet follow the fluctuations of the anisotropy axes of a crystallite group, expression (15) for the density of distribution of the effective anisotropy axes is simultaneously the statistical distribution of the magnetization vector of a stochastic magnet. The correlation breaks that can be seen in Figure 2 can be explained by the fact that the SDs are characterized by a certain spread of the effective anisotropy constants. In addition, there is a weak interaction between separate SDs. As a result, the SDs with the prevailing effective anisotropy affect the magnetization orientation of weaker domains. The exchange coupling strengthens the fragile stochastic regularity. Thus, the self-organized area arises, where the exchange coupling ensures the quasi-homogeneous magnetization. The SD structure is diverse and depends on the fabrication technique and prehistory. The SD sizes can differ by an order of magnitude. In particular, a SD shown in Figure 1 contains over three hundreds of crystallites. At the same time, at the continuous magnetization rotation, the SDs sometimes arise whose size barely reaches the domain wall thickness value.

When the magnetostatic interaction starts working, SDs become invisible. Classical domains and domain walls appear. We may mistakenly assume that switching on the uniform macroscopic anisotropy annihilates SDs and disappears the characteristic length δ_S. Meanwhile, the magnetization self-organization is observed in nanowires in the presence of the uniform macroscopic anisotropy induced by magnetostatics. Stochastic domains are analogous to the normal modes of bound oscillators, which can be excited or not, but exist as a structural unit. Below we consider some ways of obtaining the superstructure parameters.

4 Self-organization manifestation upon magnetization switching

Let the wire be magnetized in the z axis direction, i.e., along the effective anisotropy axis caused by magnetostatics. The magnetic structure is almost homogeneous, except for weak oscillations of the EMA direction. Below we show that some parts of the inhomogeneities are initial nuclei of inverse domains. The observations show that the sizes of these parts are similar to those of SDs.

We apply an external magnetic field in the direction opposite to the average magnetization. The applied field increases deviations of the magnetization from the z axis direction. The beginning of this process is illustrated in Figure 3.

When the external field attains a critical value of $H_{nucl} \approx 0.16\mu_0 M_S$, the magnetization of separate nuclei drastically rotates, which results in the occurrence of 180- or 360-degree domain walls [27]. Figure 4 illustrates the end of this process.

Upon magnetization switching of a nucleus, its spatial size remains nearly invariable. The frequently occurring

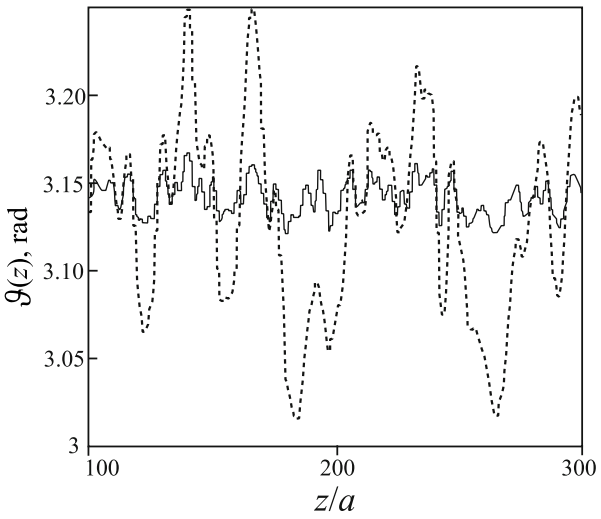

Fig. 3. Enhancement of magnetization fluctuations with an increase in the external magnetic field. The solid line corresponds to $h = 0$ and the dashed line, to – $h = 0.05$.

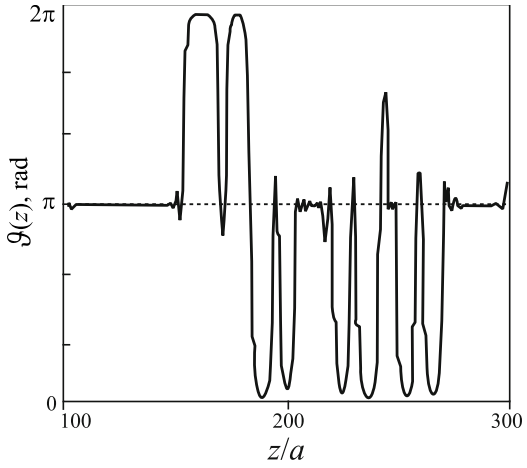

Fig. 4. Domain structure formed at attaining the critical field.

360-degree domain walls and some of 180-degree walls do not move upon variation in the external magnetic field. The low mobility originates from the fact that at large saturation magnetizations M_S of a material, the demagnetizing field creates satellite domains with the opposite magnetization at the domain edges (Fig. 4). The domain wall continuation in the satellite works as a part of the 360-degree wall, pinning the latter [27]. The nuclei domain walls are special and have the anomalously low mobility. The obtained domains are located in the places where SDs would be located if the induced magnetostatic anisotropy were absent. Thus, despite the effect of such a strong masking factor as the anisotropy induced by magnetostatics, the information about SDs is stored. The phenomenon of pinning the domain walls that separate the regions related to SDs can apparently be observed in experiments. The experiment should follow the scenario described above.

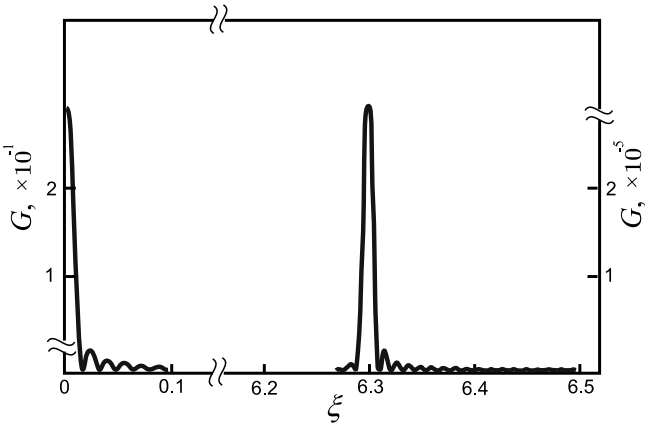

Fig. 5. Characteristic spectral density of the distribution of the polar angle for a magnet at $b = 0.1$.

5 Spectral analysis of magnetization

As was shown in the previous section, self-organization manifests itself even at the prevailing uniform anisotropy. Spectral study of the magnetization distribution function makes it possible to consider the structure in more detail without switching the sample magnetization. Let us consider the spectral density $G(\xi)$ of the spatial distribution of the polar angle $\vartheta(z)$

$$G(\xi) = \frac{1}{4\pi^2}\left(\int_0^L \vartheta(z)\cos(z\xi)dz\right)^2 + \frac{1}{4\pi^2}\left(\int_0^L \vartheta(z)\sin(z\xi)dz\right)^2. \quad (18)$$

The spatial magnetization distributions $\vartheta(z)$ shown in Figures 2 and 3 were obtained at the same implementation of the stochastic anisotropy field at different external fields. These distributions were subjected to the spectral analysis.

It can be seen that with an increase in the field, the families of functions $\vartheta(z)$ exhibit the common features. The peaks and dips in the $\vartheta(z)$ curves are positioned at the same places and only have different values. However, in the critical external fields, one can observe significant differences. The nuclei transform to domains. At the same time, it is remarkable that the spectral densities at any external field values completely coincide. The effects masking the self-organization (external field, texture in the EMA directions, magnetostatics, etc.), are not reflected in the spectral density. The form of $G(\xi)$ is determined by the primary interactions (crystallographic anisotropy and exchange), i.e., by SDs. The main contribution to the spectral density is made by the long-wavelength region. It is important that, as expected, the spectral density plot contains a noticeable maximum corresponding to the crystallite sizes (right-hand part in Fig. 5).

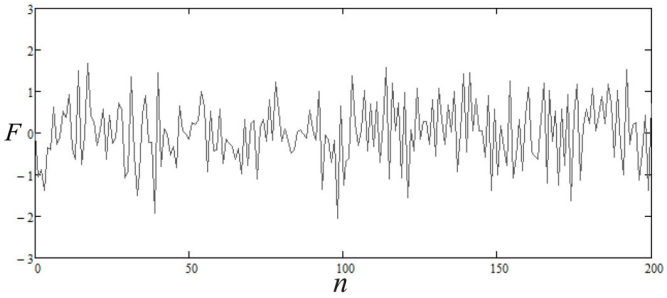

Fig. 6. Example of implementation of the pinning force for a magnet at $b = 0.04$.

The invisible domains are analogous, to a certain extent, to the observed superstructure in a bulk weak ferromagnet [28]. The main difference of SDs is their visible absence in the presence of masking factors.

6 Spectral analysis of force relief

The authors of [29–31] theoretically discussed domain wall pinning in superdispersed 1D materials on the force relief of magnetic inhomogeneities and statistical properties of this relief. They calculated the coercivity and domain wall start field are demonstrated that the average wavelength of the force relief coincides with the domain wall width. In this study, we simulated the nanowire magnetization switching in order to investigate the pinning force spectrum. The computations were made using the gradient descent technique with the initial seed magnetization distribution that initiates the formation of one stable domain wall in the nanowire. As the magnetic field applied along the z-axis was increased, the total SD energy was detected and its derivative yielded the force of interaction between the wall and inhomogeneities.

Figure 6 shows the characteristic implementation of the pinning force. Figure 7 presents the result of the spectral analysis of the force relief of wires with the same cross section and parameter $b = 0.1$, but different ratios $\mu_0 M_S^2/K$. This ensured approximately the same SD size, but different widths of domain walls between classical domains. At the values of $\mu_0 M_S^2/K$ approximately corresponding to those of iron (Fig. 6a), two pronounced spectral density maxima are observed. The maximum corresponding to the large k values is determined by the magnetization ripples upon tuning to the local anisotropy of separate crystallites. The wavelength of this ripples is about b. The other maximum is, in our opinion, complex and contains peaks responsible for the domain wall width and SD size (in this case, their characteristic sizes are comparable, i.e., the average wavelengths coincide). It can be seen from the figure that with decreasing M_S, the maximum creeps and the density peak responsible for the increasing domain wall width becomes pronounced. In this case, the peak responsible for the SD is nearly invariable.

Thus, the force relief has at least three pronounced harmonics: two long-wavelength – SD size (correlation radius of the magnetization), domain wall size with the imposed

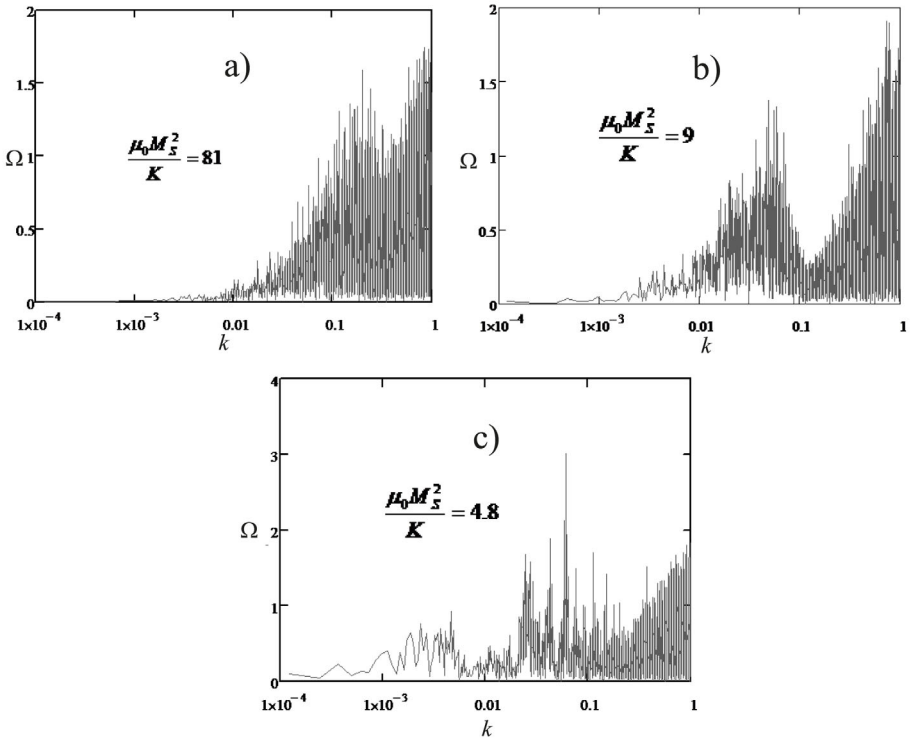

Fig. 7. Spectral density $\Omega(k)$ of the force relief for samples with different M_S values. The EMA directions are distributed randomly and uniformly over a sphere. Here, $k \approx 1/\lambda$, where λ is measured in units of a.

short-wavelength modulations – crystallite size. The domain wall width can be estimated using the expression

$$\delta_W \approx \sqrt{\frac{A}{\mu_0 M_S^2 + \mu K}} = \sqrt{\frac{A}{\frac{\mu_0 M_S^2}{K} + \mu}}. \qquad (19)$$

Here, the denominator can be interpreted as the effective uniaxial anisotropy constant along the long axis of the 1D material. As a rule, in ferromagnets the magnetostatic term prevails over the crystallographic anisotropy even in the case of the rigid texture ($\mu = 1$). Therefore, the dependence $\delta_W(\mu)$ is difficult to check. The numerical estimation of δ_W using formula (19) agrees satisfactorily with the simulation results shown in Figure 7 [26].

7 Conclusions

We reported the results of computer simulation of the properties of magnetization and relief pinning a domain wall in 1D inhomogeneous ferromagnets. The spectral analysis of magnetization allowed us to determine the long-wavelength harmonic, which is attributed by us to the existence of the so-called stochastic domains (magnetic blocks). The wavelength of this harmonic coincides with the stochastic domain size. It is noteworthy that this characteristic length manifests itself not only in the trivial manner, as in the magnetization switching process, but also in the implicit case as a result of spectral decomposition of the magnetization or force pinning the domain wall. The dependence of the wavelength of the harmonic responsible for the stochastic domain on the linear crystallite size coincides with the theoretical estimations.

It was demonstrated that the parameter characterizing the new self-organization is the induced stochastic anisotropy. We derived the universal expression for the induced stochastic anisotropy, which involves fluctuations of the crystallite size, fluctuations of the local constants, and arbitrary distribution of the local anisotropy axes directions, which explains the nucleation of a stochastic domain.

The magnetostatic interaction leads to the formation of a domain structure and, consequently, to the occurrence of one more characteristic length – the domain wall width.

Variants of experimental determination of the stochastic self-organization in the presence of a masking factor (strong induced anisotropy) were proposed.

Author contribution statement

The contributions of the two authors are equal.

Sections 2, 4–6 of the work was supported by Russian Foundation for Basic Research (RFBR), Project No. 17-02-00254-a. Section 3 was supported by Russian Science Foundation, Project No. 14-15-00805.

References

1. A.M. Goodman, S.J. Greaves, Y. Sonobe, H. Muraoka, Y. Nakamura, IEEE Trans. Magn. **38**, 2051 (2002)
2. S. Da Col, M. Darques, O. Fruchart, L. Cagnon, Appl. Phys. Lett. **98**, 112501 (2011)
3. V.N. Blinov, V.N. Buravtsev, T.I. Makarova, A.I. Poletaev, Moscow University Physics Bulletin July **68**, 299 (2013)
4. A.M. Shutyi, Techn. Phys. **56**, 1225 (2011)
5. E.V. Matizen, V.G. Martynets, P.P. Bezverkhy, *Self-organizing criticality state in the Josephson array* (Vestnik SibGUTI, 2009), pp. 137–144
6. F.V. Lisovskii, E.G. Mansvetova, J. Exp. Theor. Phys. Lett. **55**, 32 (1992)
7. G.S. Kandaurova, Physics-Uspekhi **45**, 1051
8. F.V. Lisovskii, O.P. Polyakov, J. Exp. Theor. Phys. Lett. **73**, 483 (2001)
9. N. Rougemaille, A.K. Schmid, J. Appl. Phys. **99**, 085502 (2006)
10. V.M. Prida, K.R. Pirota, D. Navas, A. Asenjo, M. Hernandez-Velez, M. Vazquez, J. Nanosc. Nanotechnol. **7**, 272 (2007)
11. V.A. Ignatchenko, J. Exp. Theor. Phys. **27**, 303 (1968)
12. Y. Imry, S.-K. Ma, Phys. Rev. Lett. **35**, 1399 (1975)
13. E.M. Chudnovsky, W.M. Saslov, R.A. Serota, Phys. Rev. B **33**, 251 (1986)
14. A.A. Ivanov, V.A. Orlov, G.O. Patrushev, The Physics of Metals and Metallography **103**, 219 (2007)
15. I.S. Edelman, L.I. Chernyshova, The Physics of Metals and Metallography **28**, 440 (1969) [in russian]
16. Y. Henry, A. Iovan, J.-M. George, L. Piraux, Phys. Rev. B **66**, 184430 (2002)
17. S.V. Komogortsev, R.S. Iskhakov, Phys. Solid State **47**, 495 (2005)
18. A.A. Ivanov, V.A. Orlov, Math. Modeling **25**, 28 (2013) [in russian]
19. A.A. Ivanov, G.O. Patrushev, The Physics of Metals and Metallography **86**, 331 (1998)
20. A.A. Ivanov, V.A. Orlov, G.O. Patrushev, Phys. Solid State **41**, 1311 (1999)
21. A.A. Ivanov, V.A. Orlov, G.O. Patrushev, N.N. Podolskii, The Physics of Metals and Metallography **109**, 120 (2010)
22. A.A. Ivanov, V.A. Orlov, G.O. Patrushev, The Physics of Metals and Metallography **102**, 485 (2006)
23. A.A. Ivanov, V.A. Orlov, The Physics of Metals and Metallography **84**, 122 (1997)
24. A.A. Ivanov, V.A. Orlov, G.O. Patrushev, Phys. Solid State **51**, 762 (2009)
25. I.V. Lobov, The Physics of Metals and Metallography **61**, 817 (1986) [in russian]
26. A.A. Ivanov, V.A. Orlov, Self-organization of the magnetization in ferromagnetic nanowires, J. Magn. Magn. Mater., `dx.doi.org/10.1016/j.jmmm.2016.12.053` (in Press)
27. A.A. Ivanov, V.A. Orlov, Phys. Solid State **57**, 2204 (2015)
28. A.A. Karaev, B.Yu. Sokolov, Yu.M. Fedorov, Phys. Solid State **42**, 2097 (2000)
29. A.A. Ivanov, V.A. Orlov, Phys. Solid State **53**, 2441 (2011)
30. A.A. Ivanov, V.A. Orlov, The Physics of Metals and Metallography **111**, 554 (2011)
31. A.A. Ivanov, V.A. Orlov, N.N. Podolsky, Solid State Phenomena **168-169**, 230 (2011)